Vapor-Phase Polymerization of Nanofibrillar Poly(3,4-ethylenedioxythiophene) for Supercapacitors

Julio M. D'Arcy,[†,‡] Maher F. El-Kady,[§,⊥] Pwint P. Khine,[§] Linghong Zhang,[§] Sun Hwa Lee,[†,‡] Nicole R. Davis,[†,‡] David S. Liu,[†,‡] Michael T. Yeung,[§] Sung Yeol Kim,[†,‡,∥] Christopher L. Turner,[§] Andrew T. Lech,[§] Paula T. Hammond,[†,‡,*] and Richard B. Kaner[§,¶,*]

[†]Department of Chemical Engineering and [‡]The David H. Koch Institute for Integrative Cancer Research, Massachusetts Institute of Technology, Cambridge, Massachusetts 02139, United States, [§]Department of Chemistry and Biochemistry, and California NanoSystems Institute, University of California, Los Angeles, California 90095, United States, [⊥]Department of Chemistry, Faculty of Science, Cairo University, Giza 12613, Egypt, [∥]School of Mechanical Engineering, Kyungpook National University, 80 Daehak-ro, Buk-gu, Daegu, South Korea 702-701, and [¶]Department of Materials Science, University of California, Los Angeles, California 90095, United States

ABSTRACT Nanostructures of the conducting polymer poly(3,4-ethylenedioxythiophene) with large surface areas enhance the performance of energy storage devices such as electrochemical supercapacitors. However, until now, high aspect ratio nanofibers of this polymer could only be deposited from the vapor-phase, utilizing extrinsic hard templates such as electrospun nanofibers and anodized aluminum oxide. These routes result in low conductivity and require postsynthetic template removal, conditions that stifle the development of conducting polymer electronics. Here we introduce a simple process that overcomes these drawbacks and results in vertically directed high aspect ratio poly(3,4-ethylenedioxythiophene) nanofibers possessing a high conductivity of 130 S/cm. Nanofibers deposit as a freestanding mechanically robust film that is easily processable into a supercapacitor without using organic binders or conductive additives and is characterized by excellent cycling stability, retaining more than 92% of its initial capacitance after 10 000 charge/discharge cycles. Deposition of nanofibers on a hard carbon fiber paper current collector affords a highly efficient and stable electrode for a supercapacitor exhibiting gravimetric capacitance of 175 F/g and 94% capacitance retention after 1000 cycles.

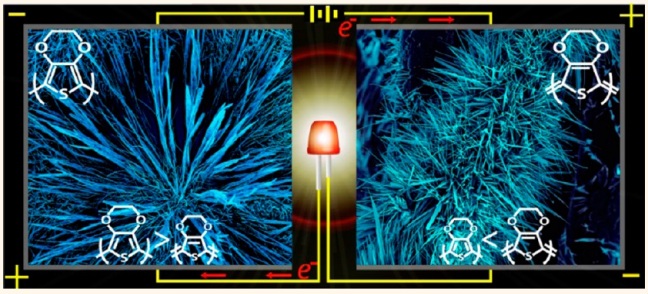

KEYWORDS: supercapacitor · vapor-phase polymerization · poly(3,4-ethylenedioxythiophene) · nanofibers · conducting polymer

Supercapacitors are electrochemical energy storage devices that provide on-demand high power density and represent an important technology that complements new sustainable energy sources.[1] A supercapacitor is composed of a highly stable electrode that can be cycled thousands of times without affecting energy storage efficiency, thereby enabling extended device lifetime.[2] In order to rapidly store or deliver current, the electrode requires a capacitive material such as a transition metal oxide, carbon allotrope, conducting polymer, or a mixture thereof.[1,3] Among these materials, a conducting polymer is an attractive candidate due to its excellent solution-based processability, reversibility between redox states, and metallic conductivity.[4−6] A conducting polymer supercapacitor is actually a pseudocapacitor; however, by convention, this device is also referred to as a supercapacitor. The conducting polymer poly(3,4-ethylenedioxythiophene) (PEDOT) possesses the highest conductivity (4500 S/cm) among all conducting polymers, albeit only when deposited from the vapor phase.[7] Deposition of PEDOT from the vapor phase is compatible with most electrode materials and leads to strong adhesion between polymer and current collector. In spite of these advantages, the majority of state-of-the-art symmetric supercapacitors are based on electrochemically deposited PEDOT,[3−5,8] a highly capacitive

* Address correspondence to hammond@mit.edu, kaner@chem.ucla.edu.

Received for review October 26, 2013 and accepted January 14, 2014.

Published online February 03, 2014
10.1021/nn405595r

material. Solution-based oxidation of PEDOT, on the other hand, typically leads to supercapacitors with a specific capacitance lower than 150 F/g; a notable exception of 400 F/g sadly renders the supercapacitor electrode unstable in water.[9]

Electrochemical deposition affords intimate electrical contact leading to low contact resistance between polymer and current collector and is therefore a popular synthetic strategy for developing a state-of-the-art symmetric PEDOT supercapacitor.[4] Although some high-performance results were obtained,[4−8] the PEDOT electrodes were only several hundreds of nanometers in thickness, leading to low areal capacitance that is not suitable for practical applications.[10] Furthermore, supercapacitors produced from this technique suffer from poor chemical and cycling stability, another problem that limits the versatility of PEDOT supercapacitors.

The vapor-phase deposition of PEDOT is a new strategy that is underutilized in the fabrication of supercapacitors. Earlier work in vapor-phase deposition demonstrates a templated route to a nanofibrillar PEDOT supercapacitor disappointedly possessing low specific capacitance of 20 F/g and low conductivity of 60 S/cm.[11] Current vapor-phase research efforts lead to bulk PEDOT, a supercapacitor with specific capacitance of 92 F/g, and a highly conductive form of the polymer (140 S/cm).[2] Here we demonstrate a state-of-the-art supercapacitor composed of a high packing density of one-dimensional PEDOT nanostructures deposited from the vapor phase on hard carbon fiber paper current collectors. The PEDOT film is 20 μm thick, comparable to the thickness of electrodes commonly used in commercially available supercapacitors, making it potentially useful for practical applications. This symmetric supercapacitor is characterized by high capacitance (175 F/g), high conductivity (130 S/cm), and excellent electrochemical stability, retaining 92% capacitance after 10 000 cycles. Advantageously, high aspect ratio PEDOT nanofibers deposit from the vapor phase without the need for a prefabricated extrinsic template.

PEDOT's long-term environmental stability, narrow band gap,[7] and high electrical conductivity[12] afford an ideal prototypical organic material for electrochromic,[13] solar cell,[14,15] and fuel cell applications[16] as well as supercapacitors. Electrochemical charge storage in PEDOT is a surface phenomenon that strongly depends on the electrical conductivity and surface area of the polymer electrode.[1,2,4,6] Here, high aspect ratio nanofibrillar morphology increases the surface area of the polymer active layer, optimizes surface-based electronic properties, and enhances current transport.[17,18] The growing importance of one-dimensional morphologies in conducting polymers has driven innovation and discovery of a plethora of strategies for synthesizing PEDOT nanofibers. Three common approaches are solution-based oxidation,[15] electrochemical synthesis,[19] and vapor-phase deposition.[12,20] However, until now, high aspect ratio PEDOT nanofibers could only be deposited from the vapor-phase utilizing templates such as anodized aluminum oxide or pre-electrospun nanofibers which lead to a material of low conductivity and require postsynthetic template removal. Such conditions stifle the development of conducting polymer electronics.

Among the various protocols, vapor-phase deposition is an attractive candidate because it leads to a highly conductive thin film of PEDOT characterized by smooth and flat nanoscale morphology.[7,21] The exceptionally high uniformity, optoelectrical stability, and low optical density of a vapor-deposited film make this synthetic strategy a powerful tool[12] (see Supporting Information). Attempts at direct nontemplated deposition of PEDOT nanoarchitectures from the vapor phase have unfortunately resulted in low aspect ratio nanostructures such as dendritic snowflakes,[7] as well as low conductivity nanobowls[21] and basalt-like nanopores.[18] Deposition of high aspect ratio nanostructures occurs from the vapor phase with the assistance of prefabricated electrospun nanofibrillar templates; however, PEDOT nanofibers suffer from low electrical conductivity. A uniform array of high aspect ratio nanobundles can also be deposited from the vapor phase by utilizing anodized alumina oxide as an extrinsic hard template.[22] However, these templates need to be removed and require an additional postsynthetic step.[23−25]

Here we demonstrate an innovative, simple, and direct route to both high conductivity and high aspect ratio architectures of PEDOT from the vapor phase, obviating the need for template removal. Our protocol is an evaporative vapor-phase polymerization (EVPP) that results in a robust thick freestanding film composed of a vertically directed anisotropic nanoscale architecture that peels off of a substrate and can serve as the active layer in an electrochemical supercapacitor. This strategy advances the state-of-the-art by demonstrating that vapor-phase deposition is a facile and powerful technique for directly depositing high aspect ratio one-dimensional nanostructures.

RESULTS AND DISCUSSION

EVPP is carried out at ambient pressure inside a chemical vapor deposition chamber (Supporting Information Figure S1) utilizing an aqueous microdroplet of oxidant ($FeCl_3$) placed on a gold-coated substrate under an atmosphere of chlorobenzene vapor carrying the monomer (ethylenedioxythiophene) (Figure 1a). The temperature is ramped up from 25 to 130 °C at approximately 400 °C/h, reaching 130 °C within 12 min, and is kept at 130 °C for 33 min (Figure S2). This 45 min polymerization results in a disk-shaped PEDOT film with a 1 cm diameter (Figure 1b) characterized by a highly texturized topography, as shown by optical microscopy (Figure 1c).

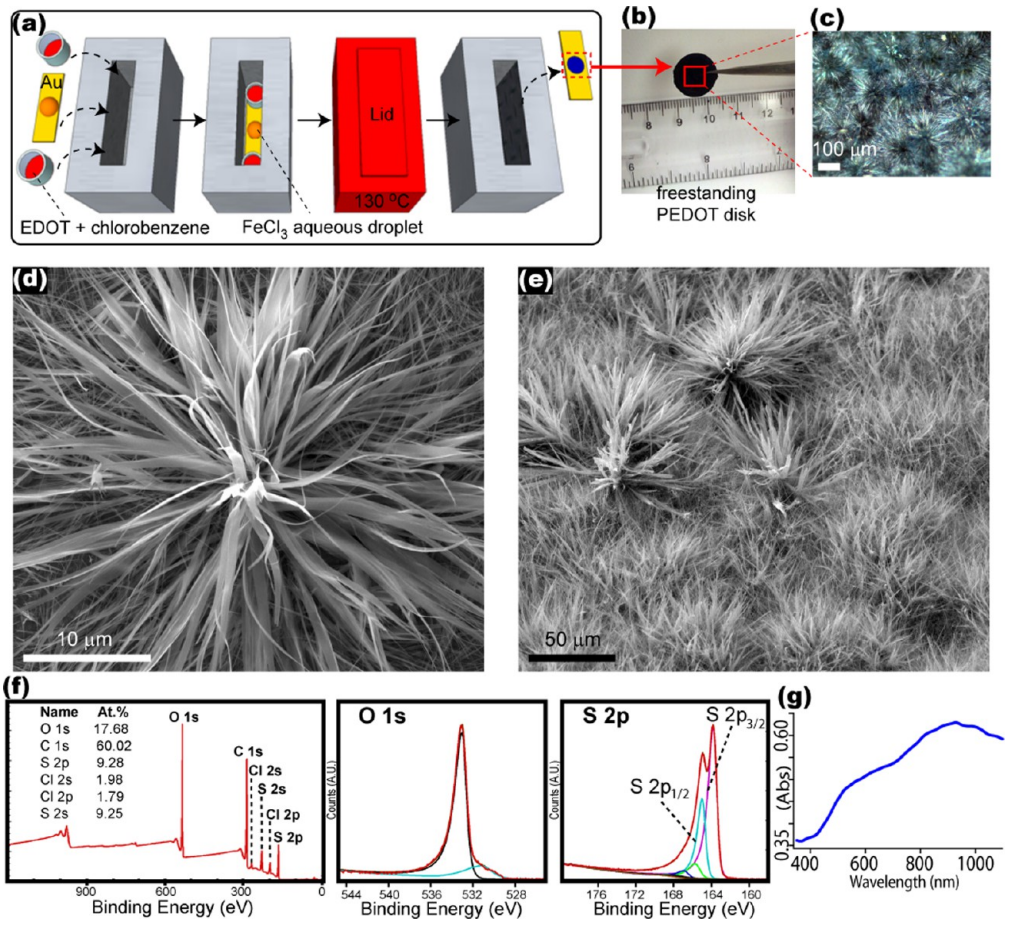

Figure 1. Evaporative vapor-phase polymerization (EVPP) leads to high aspect ratio PEDOT one-dimensional nanoribbons and nanofibers. (a) Flow-process diagram of EVPP-PEDOT nanofibers shows oxidant droplet's color change from orange to blue during polymerization. (b) Final product is a mechanically robust freestanding disk-shaped film that is approximately 1 cm in diameter and can be easily picked up using tweezers. (c) Low-magnification optical microscopy shows this blue colored disk-shaped film is composed of highly texturized vertically directed anisotropic one-dimensional architectures. (d) Top view scanning electron micrograph (SEM) of EVPP-PEDOT shows vertically directed high aspect ratio nanoribbons. (e) Low-magnification tilted SEM image shows large-scale morphology composed of a high packing density of vertically directed high aspect ratio nanofibers and nanoribbons. (f) Chemical composition of EVPP-PEDOT is determined using X-ray photoelectron spectroscopy and elemental analysis. The elemental analysis shows a C/S ratio of 6.4 that is in close agreement with the expected theoretical value of 6.0 for PEDOT. The high-resolution peaks for O1s and S2p have the correct intensity, shape, and position. (g) UV−vis absorption spectrum for EVPP-PEDOT is characterized by a metallic state that is typical of a highly doped and conductive form of PEDOT.

A scanning electron micrograph (SEM) of a free-standing film of EVPP-PEDOT shows that the final product is characterized by a topography composed of wrinkles that are up to 50 μm in width and up to 1 mm in length (Figure S3). These wrinkles are densely coated by high aspect ratio vertically directed one-dimensional rigid nanoribbons (Figure 1d and Figure S4a,b) that are up to 5 μm in diameter and up to 100 μm in length and by high aspect ratio vertically directed nanofibers that are up to 250 nm in diameter and up to 10 μm in length (Figure 1e and Figure S4c,d). Dimensional analysis of SEM images shows nanoribbons composed of bundles of nanofibers with an aspect ratio of up to 250 (Figure S4e,f).

Spectroscopic analysis for a washed sample (see Supporting Information) shows that the chemical composition of EVPP-PEDOT is typical of PEDOT as determined by X-ray photoelectron spectroscopy (XPS) (Figure 1f). Characteristic bonding in the O1s region associated with the dioxane ring appears at 533.2 eV and can be assigned to the oxygen ether group (C−O−C), while the peak at 531.7 eV (C−O) pertains to PEDOT in the doped state.[26] The spin-sulfur coupling, $S2p_{3/2}$ (163 eV) and $S2p_{1/2}$ (165 eV), is also present.[19] An EVPP-PEDOT film contains a negligible amount of iron and possesses a Cl/S ratio of 0.2 due to the counteranion Cl^- when doped.[27] Atomic concentrations demonstrate a C/S ratio of 6.4 that is typical for PEDOT[28] and in close agreement with its theoretical value of 6.0; this minor discrepancy is possibly due to adventitious hydrocarbon contamination. Extensive probe sonication of EVPP-PEDOT in chlorobenzene leads to fragmentation and affords a colloidal dispersion for ultraviolet−visible (UV−vis) absorption spectroscopy

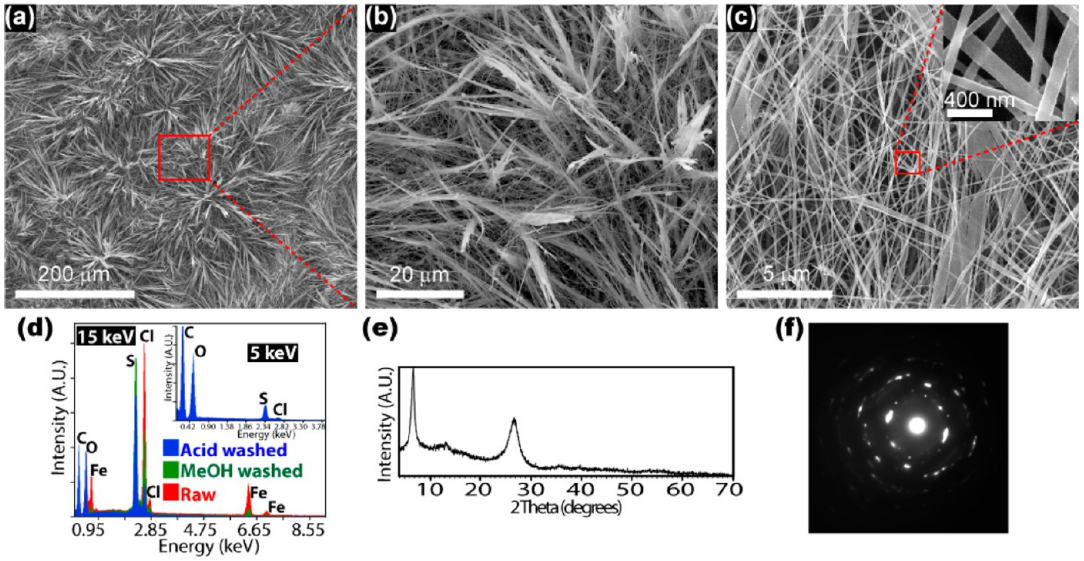

Figure 2. Structural analysis of EVPP-PEDOT. (a,b) Close-up sequence of SEM images demonstrates a high packing density of both vertically directed high aspect ratio nanoribbons and nanofibers. (c and Inset) Top view SEM image shows nanofibers entangled with nanoribbons that possess a diameter of up to 200 nm. (d) Energy-dispersive X-ray spectroscopy demonstrates that iron is present in EVPP-PEDOT after the methanol wash (green); however, this metal is undetectable after washing with acid (blue). (e) X-ray powder diffraction of an EVPP-PEDOT shows an intense (100) peak due to preferential orientation of polymer chains on a gold substrate. (f) Electron diffraction confirms that EVPP-PEDOT is a polycrystalline material.

(Figure 1g) showing a $\pi-\pi^*$ transition in the 650 nm region associated with the conductive metallic state for PEDOT.[29]

Unlike traditional vapor-phase deposition protocols that require a dry and homogeneous precoat of the oxidant, EVPP is simpler and requires only pipetting of the aqueous oxidant droplet on a substrate (see Methods and Supporting Information). EVPP is a rapid versatile process that leads both to freestanding films and to conductive nanofibrillar coatings on various substrates. One-dimensional nanostructures of EVPP-PEDOT deposit as the oxidant droplet evaporates, inducing precipitation of anisotropic $FeCl_3$ crystallites that serve as both nucleation sites and intrinsic templates (Figure S5). This dual role for $FeCl_3$, as oxidant and intrinsic template, is an integrated advantage making nanofibrillar deposition a simple process. Controlling the precipitation of $FeCl_3$ microcrystals directs the formation of nanofibers and nanoribbons. The reduced oxidant is purified by rinsing in methanol and/or in a 1−6 M HCl aqueous solution.

A homogeneous film composed of high packing density of vertically directed high aspect ratio nanostructures can be repeatedly deposited and patterned from run to run. Maintaining a constant droplet diameter during evaporation controls both the density of nucleation and area of deposition leading to reproducible nanofibrillar morphology. In order to sustain a constant diameter, the point of contact of a droplet between air, liquid, and solid is anchored by droplet/substrate interactions that arise from surface roughness and chemical heterogeneities in a process known as pinning (see Supporting Information). Various substrates such as glass, quartz, silicon, silicon dioxide, mica, indium tin oxide coated glass, highly oriented pyrolytic graphite, tin metal, and gold-coated surfaces were tested. Silica, metal oxides, and freshly cleaved silicate substrates lead to complete droplet spreading of an oxidant droplet due to their hydrophilic properties; graphite presents a hydrophobic surface that leads to droplet beading. All of these substrates require tailoring of their surface energy *via* chemical treatment, making pinning and high aspect ratio nanostructures difficult to control, whereas tin reacts with $FeCl_3$, resulting in an amorphous polymer morphology. Only the gold-coated substrate provided a reproducible pinning mechanism.

Placing an aqueous droplet of $FeCl_3$ on a gold surface etches the coinage metal even at room temperature and leads to the formation of Au(I) species in solution.[30] Droplet pinning results from the formation of solutes during chemical etching of the gold substrate[31] and from the accumulation of solids during evaporation.[32] $FeCl_3$ crystallites present at the droplet/substrate interface are reduced to $FeCl_2$ during polymerization (Figure S6); both of these solids induce pinning. Utilizing a gold substrate therefore affords a constant contact area mode of evaporation, a disk-shaped film (Figure S7), and a homogeneous large-scale topography of vertically directed high aspect ratio nanoribbons and nanofibers (Figure 2a−c, inset). Replacing $FeCl_3$ with $HAuCl_4$ (chloroauric acid) results in an over oxidized brown material that lacks nanofibers likely because of its higher standard oxidation potential (E_0 = +1.50 eV) compared to that of $FeCl_3$ (E_0 = +0.77 eV).

Throughout the first stages of deposition, a blue polymer skin forms at the edge of the evaporating droplet; this smooth and hardened exterior shell grows radially inward as the reaction progresses, thereby enveloping the droplet's central portion (Figure S8). Within the first 15 min of polymerization, the majority of the sample becomes wet and coated by hollow protrusions (Figure S9a); these grow in size and number as the polymerization progresses (Figure S9b,c). Hollow structures span a diameter ranging from 500 nm to 1 μm and form as the oxidant aqueous solution evaporates through the hardened polymer shell. During polymerization, the deposition chamber is saturated with chlorobenzene vapors carrying monomer molecules. The contact of chlorobenzene with an aqueous oxidant droplet leads to an interfacial surface tension gradient. Hollow protrusions are the result of surface free energy minimization as the aqueous oxidant solution evaporates, diffuses, and polymerizes through the chlorobenzene/monomer-coated hardened polymer shell. Other solvents were also tested such as dimethylformamide, toluene, dichloromethane, chloroform, carbon tetrachloride, and 1,2-dichlorobenzene; however, only chlorobenzene led to high aspect ratio nanofibers possessing high conductivity. Chlorobenzene is a low surface tension (33 mN/m) halogenated aromatic solvent that can dissolve low molecular weight thiophene oligomers and is characterized by a sufficiently low boiling point (130 °C) for vapor-phase synthesis without causing polymer degradation.

The role of oxidant concentration was tested with 0.0266, 0.0532, 0.133, 0.266, 0.532, and 1.33 M aqueous solutions of $FeCl_3$ utilizing a 150 μL droplet. The nanofibrillar aspect ratio increased proportionally with concentration up to 0.266 M, while a 2-fold increase led to aggregation, and 1.33 M resulted in complete stifling of nanofibrillar growth. Keeping the concentration constant (0.266 M) and using a larger droplet (1000 μL) led to a thinner film of wider diameter that suffered from brittleness. EVPP-PEDOT lacked nanostructures when excess water vapor was introduced into the CVD chamber (Figure S10) or when $FeCl_3$ was replaced with iron(III) *p*-toluenesulfonate. Alternatively, a partially dried oxidant droplet produced an aggregated morphology, but after rehydration inside a humidity chamber, it yielded both nanofibers and aggregates. A rehydrated droplet does not regain its original spherical shape and is characterized by a heterogeneous distribution of oxidant and water; a relative humidity ranging between 35 and 65% is necessary for synthesizing high-quality PEDOT nanofibers[26] (see Supporting Information).

Energy-dispersive spectroscopy shows that EVPP-PEDOT nanostructures deposit on an underlying oxidant intrinsic template (Figure S11) that can be partially dissolved by methanol (Figure 2d, green line) and completely removed in a hydrochloric acid solution (Figure 2d, blue line) during purification. Removal of the intrinsic template relaxes the architecture and induces entanglement between nanofibers and nanoribbons (see Supporting Information, Figure S12). A washed EVPP-PEDOT film (see Supporting Information) has crystallites with a preferred orientation as demonstrated by X-ray powder diffraction (Figure 2e). The peak centered at 6.7° 2θ is characteristic of the (100) spacing due to the interchain distance between layers of π-stacked chains ranging between 1.33 and 1.39 nm for Cl^--doped PEDOT. The peak at 26.7° 2θ is due to the face-to-face packing distance between chains and is in the 0.3−0.4 nm range;[19,33] EVPP-PEDOT is a polycrystalline material as demonstrated by electron diffraction (Figure 2f).

Temperature *versus* sheet resistance was studied by carrying out syntheses at 70, 80, 90, 110, and 130 °C, resulting in film sheet resistances at 45 min of 300, 300, 180, 50, and 5 Ω/square, respectively. A substrate temperature above 100 °C increases the reaction rate of polymerization, promoting deprotonation and the evaporation of scavenged protons as HCl; this minimizes acid-catalyzed side reactions that can degrade the polymer structure, resulting in a longer conjugated backbone and higher conductivity.[12] The conductivity of a washed sample (see Supporting Information) was determined by two-probe current−voltage (*I*−*V*) measurements (Figure 3a) as well as by a four-point probe configuration using a thickness of 20 μm as determined *via* profilometry (Figure 3a, bottom right). The sheet resistance of an EVPP-PEDOT film is at least 5 times lower than flexible fabrics coated with vapor-phase PEDOT.[25] The conductivity of a disk-shaped freestanding film of EVPP-PEDOT is 130 S/cm and superior to templated PEDOT grown on electrospun nanofibers of polyacrylonitrile or poly(vinyl alcohol) with corresponding values of 1−8[23] and 61 S/cm,[24] respectively.

Analysis of nonwashed (black) and methanol-washed (green) EVPP-PEDOT samples shows a difference in their Raman spectra (excitation wavelength 676 nm) (Figure 3b). Both samples exhibit a strong absorption in the 1423 cm^{-1} region that is characteristic of symmetric C_α═C_β(−O) stretching and indicative of a high level of oxidation.[34] Broadening of the 1501 cm^{-1} asymmetric C═C stretching mode is characteristic of alcohol-washed PEDOT.[35] The band from the C_β−C_β stretch at 1365 cm^{-1}, the inter-ring stretch at 1264 cm^{-1}, and the oxyethylene ring deformation peak at 990 cm^{-1}, as well as the C_α−$C_{\alpha'}$ inter-ring stretch at 1257 cm^{-1} are all characteristic of PEDOT.[24] The Fourier transform infrared spectrum (Figure 3c) shows a C═C peak at 1523 cm^{-1} due to conjugation, indicating high conductivity.[35]

The properties of EVPP-PEDOT look promising for many applications. In particular, the high electrical

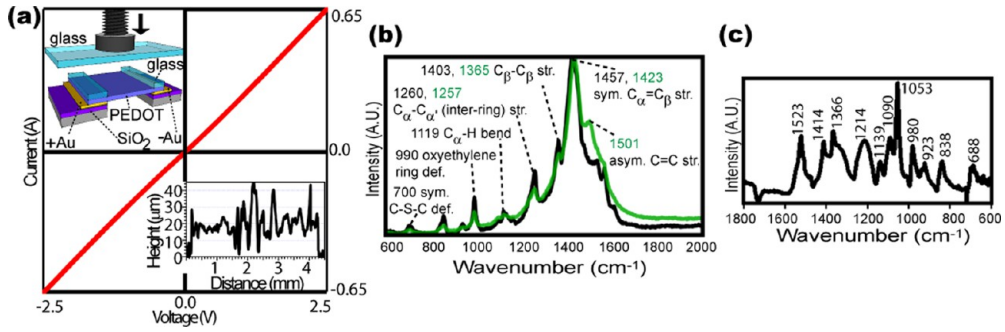

Figure 3. Conductivity and spectroscopic characterization. (a) Current−voltage (*I*−*V*) curve of EVPP-PEDOT is measured by (top left) clamping gold electrodes on a squared freestanding film. Utilizing an average film thickness of 20 μm as determined *via* profilometry (bottom right) leads to a conductivity of 130 S/cm; this value is corroborated by utilizing four-point probe geometry. (b) Overlapped Raman spectra of nonwashed (black) and methanol-washed (green) samples show characteristic asymmetric (1501 cm^{-1}) and symmetric stretches (1457 and 1423 cm^{-1}) associated with a doped conductive state. (c) Fourier transform infrared spectrum shows broad absorption peaks between 1450 and 700 cm^{-1} and a C═C peak at 1523 cm^{-1}, indicative of conjugation.

conductivity, surface area, and electron mobility are interesting for energy conversion and storage applications.[20,36−38] Among various energy storage devices, supercapacitors have recently attracted significant attention due to their high power density and long cycling stability.[39] PEDOT supercapacitors store charges *via* fast and reversible redox reactions (doping and dedoping) occurring primarily at the surface of PEDOT electrodes.[1] However, the limited conductivity and surface area of a conventional formulation such as PEDOT poly(styrenesulfonate) (PSS) has limited the charge storage capacity of PEDOT supercapacitors, thus precluding their widespread application. The nanostructured architecture of EVPP-PEDOT along with its high surface area and high electrical conductivity could provide a solution to this problem. To test the performance of washed EVPP-PEDOT (see Methods section) films in supercapacitors, a device was fabricated as shown in Figure 4a. Unlike PEDOT/PSS, the EVPP-PEDOT supercapacitor shows near ideal rectangular cyclic voltammogram (CV) profiles, indicating excellent capacitive behavior and low internal resistance (Figure 4b).[1] Facile electron and ion transport kinetics result in fast electrochemical switching and highly reversible doping/dedoping reactions that lead a PEDOT pseudocapacitor to behave capacitively.[2,3,6,9] Remarkably, the nanostructured EVPP-PEDOT supercapacitor exhibits about 3 times the capacity of bulk PEDOT/PSS (Figure 4c). These conclusions were also confirmed from the galvanostatic charge/discharge (CD) curves (Figure 4d). The EVPP-PEDOT supercapacitor shows nearly ideal triangular CD curves with only a small voltage drop at the beginning of each discharge curve, which again confirms superior capacitive behavior. These linear and symmetric CD curves are characteristic of PEDOT pseudocapacitors possessing high Coulombic efficiency and excellent reversibility.[2,6,11] Furthermore, the EVPP-PEDOT supercapacitors can be operated at high charge/discharge rates without suffering any significant loss in their charge storage capacity. For example, Figure 4e shows that an EVPP-EPDOT supercapacitor can be operated at charge/discharge rates that are 100 times faster, while maintaining more than 83% of its full capacity. Meanwhile, a PEDOT/PSS supercapacitor can only maintain 39% of its capacity when operated under the same conditions.

The improved rate capacity of the EVPP-PEDOT supercapacitor can be explained by the short ionic diffusion pathway during the charge/discharge processes (Figure 4f). Charging the bulk of PEDOT/PSS electrodes requires the transport of ions into the bulk of the electrode material, resulting in a slow charge/discharge process. In contrast, the nanoscale architecture of EVPP-PEDOT facilitates ion transport kinetics. As a result, a high charge storage capacity and fast charge/discharge performance can be achieved with an EVPP-PEDOT supercapacitor. A comparison of the energy density and power density of the tested PEDOT supercapacitors is presented in a Ragone plot shown in Figure 4g. The nanostructured EVPP-PEDOT supercapacitor exhibits both higher energy and power densities when compared to a conventional PEDOT/PSS supercapacitor. Moreover, the EVPP-PEDOT supercapacitor shows excellent cycling stability, retaining more than 92% of its initial capacitance after 10 000 charge/discharge cycles (Figure 4h). The image in Figure 4i demonstrates a practical application where an EVPP-PEDOT supercapacitor is used to light up a red LED for 5 min (Supporting Information movie S1). Notably, EVPP-PEDOT films are freestanding and mechanically robust and are used directly as supercapacitor electrodes without the need for organic binders or conductive additives generally used in conventional supercapacitors.

In order to increase gravimetric capacitance, the device geometry is re-engineered by directly depositing the active PEDOT layer on a current collector from the vapor phase. This synthetic strategy increases interfacial adhesion and reduces ohmic loss. Evaporative vapor-phase polymerization is carried out by

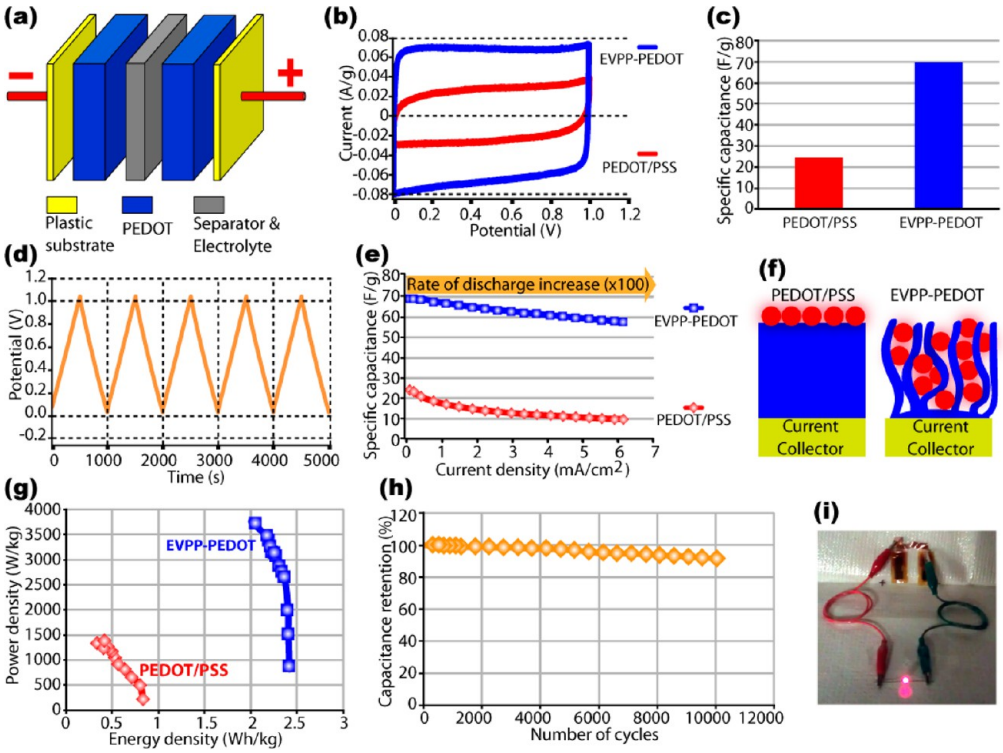

Figure 4. Fabrication of EVPP-PEDOT supercapacitors. (a) Schematic diagram of supercapacitor structure; each electrode has a mass of 1.5 mg. (b) Cyclic voltammograms (CVs) show the performance of EVPP-PEDOT supercapacitor at 2 mV/s; the performance of conventional PEDOT poly(styrenesulfonate) (PSS) supercapacitors is also displayed for comparison. (c) Average specific capacitance values as extracted from CVs demonstrate that EVPP-PEDOT exhibits a storage capacity of 70 F/g compared with only 24 F/g for PEDOT/PSS. (d) Galvanostatic charge/discharge (CD) curves for EVPP-PEDOT supercapacitor at a current density of 0.2 mA/cm^2. (e) Specific capacitance values of the tested supercapacitors (n = 5) at different charge/discharge rates. (f) (Right) Schematic diagram of ion transport during the charging of the different PEDOT supercapacitors illustrates how EVPP-PEDOT's architecture can increase the active surface area of the electrode and maximizes ion access. (g) Energy density and power density of the different supercapacitors. (h) Cycling stability of an EVPP-PEDOT supercapacitor, tested for 10 000 cycles at a current density of 1.8 mA/cm^2. (i) Two supercapacitors connected in series and charged up at a constant voltage of 2 V for a few seconds are able to light up a red light emitting diode (LED) for 5 min.

placing a droplet of an oxidant aqueous solution on a current collector and by heating to 130 °C. These corrosive conditions oxidize current collectors, such as nickel foam, aluminum foil, as well as steel mesh, and result in non-nanofibrillar bulk PEDOT. Inorganic carbons such as amorphous particles, graphite, and carbon fibers are, on the other hand, inert materials compatible with EVPP's synthetic conditions and can be readily coated with nanofibers. Additionally, high electrical conductivity makes many of the inorganic carbons ideal materials for current collectors. Among them, carbon fiber paper is an attractive candidate, affording a stable, mechanically robust, and three-dimensional surface area that maximizes PEDOT/electrolyte interface.[4] Deposition on carbon fiber paper results in a thin nanofibrillar polymeric coating that covers only the surface of the current collector in direct contact with the oxidant solution. During synthesis, oxidant solution diffuses down and through the porous current collector resulting in a thick film of EVPP-PEDOT at the bottom of the evaporation chamber. A thin nanofibrillar coating on a three-dimensional current collector improves material utilization, maximizes surface area of electrochemical interaction, and leads to a higher capacitance.[1]

Similar to EVPP-PEDOT deposition on gold, controlling the spreading of the oxidant droplet on a current collector induces nucleation, patterns deposition, and leads to a homogeneous coating from run to run. The uniformity of deposition is crucial for reproducibility and repeatability of electrochemical experiments. Nanofibrillar deposition is controlled by patterning the placement of the oxidant droplet on the carbon fiber paper utilizing a 5 min epoxy mask that restricts droplet spreading. The epoxy affords a chemically and physically stable dielectric for corrosive electrolytes. By restricting the number of nucleation events during polymerization, EVPP results in a homogeneous coating of high packing density of vertically directed nanofibers. The epoxy coating is a simple strategy that ensures control of nanostructure deposition, synthetic repeatability, and results in a uniform and patternable nanofibrillar coating.

Scanning electron microscopy aids the study of morphology evolution during evaporative vapor-phase polymerization of PEDOT on a hard carbon fiber paper current collector. SEM images of a reaction

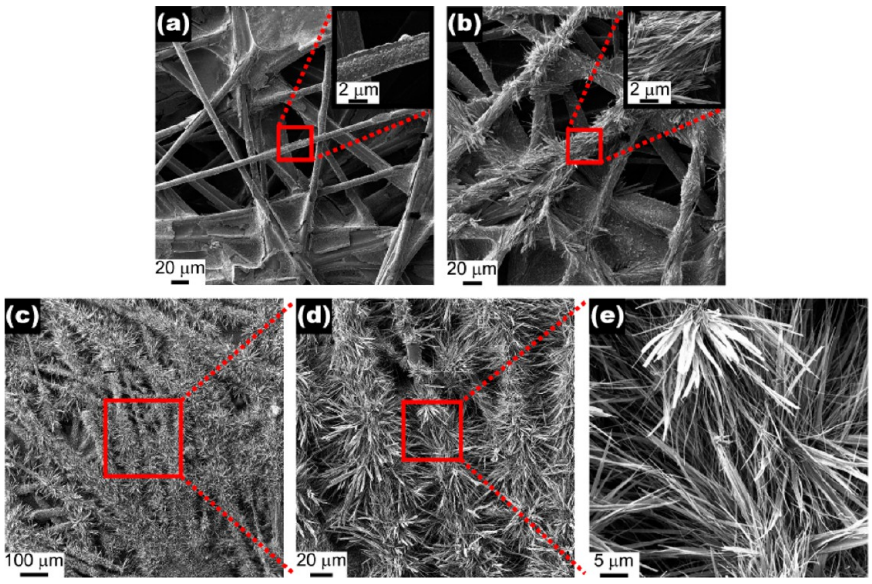

Figure 5. Helium ion micrographs (HIM) show the morphological evolution of nanofibrillar EVPP-PEDOT on a hard carbon fiber paper current collector. (a) During the first 10 min of evaporative vapor-phase polymerization, the majority of the surface layer of the carbon fiber paper current collector is coated by small particles of EVPP-PEDOT. (b) At 20 min, these small particles have grown into low aspect ratio nanofibers. Note that only the surface carbon fibers of the current collector are coated with nanofibers. (c,d) Sequence of HIM images at 45 min shows the architecture of the current collector. (c) Large-scale deposition of carbon fiber paper is homogeneous and composed of high aspect ratio PEDOT architectures characterized by (d) high packing density of one-dimensional microstructures and (e) nanostructures.

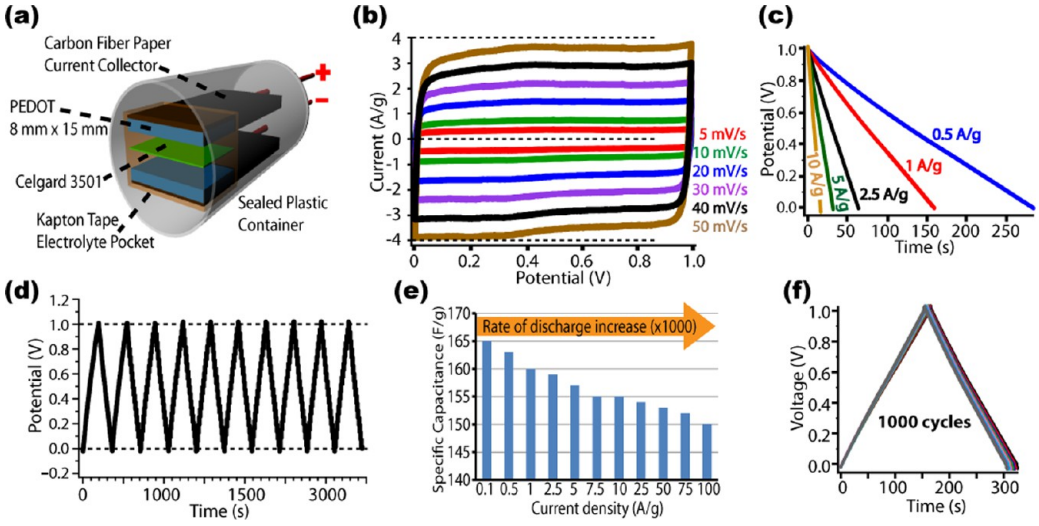

Figure 6. Fabrication of high-performance supercapacitors composed of nanofibrillar EVPP-PEDOT on hard carbon fiber paper current collectors. (a) Schematic diagram of supercapacitor structure shows a sealed plastic container and electrodes separated by a single layer of Celgard 3501. A 5 min epoxy coat protects the electrical connections from the corrosive nature of a 6 M HCl aqueous electrolyte. (b) Cyclic voltammograms at scan rates ranging between 5 and 50 mV/s and with a potential window of 1 V. The specific capacitance extracted from CVs shows a storage capacity of 175 F/g at 5 mV/s for a 0.45 mg EVPP-PEDOT mass. (c) Discharge curves at various current densities show a linear and ideal capacitive behavior as well as a specific capacitance of 160 F/g at 1 A/g current density. (d) Galvanostatic charge/discharge cycles at current density of 1 A/g show ideal reversible behavior *via* triangular-shaped plot. (e) Rate-dependent specific capacitance shows that a 1000-fold increase in the current density lowers the capacitance by only 9%. (f) A 94% capacitance retention after 1000 charge/discharge cycles at a current density of 1 A/g demonstrates the excellent electrochemical stability of EVPP-PEDOT.

quenched at 10 min of initiating polymerization show the carbon fiber paper current collector coated by small particles of polymer (Figure 5a). At 20 min, low aspect ratio nanofibers have begun to coat the surface of the current collector (Figure 5b). At 45 min, the entire surface of the current collector is coated (Figure 5c), and this large-scale deposition is characterized by a high packing density of high aspect ratio EVPP-PEDOT nanofibers (Figure 5d,e).

A high-performing supercapacitor is composed of a sealed and robust plastic cell housing two symmetric washed EVPP-PEDOT nanofiber-coated carbon fiber

current collectors (Figure 6a). This cell utilizes a 6 M HCl aqueous electrolyte that provides high ionic conductivity, low resistance, and increases the rate of charge/discharge for reversible processes such as doping and dedoping in a conducting polymer. Rectangular cyclic voltammetric plots demonstrate near ideal capacitance behavior at different scan rates under constant sweeps by showing equivalent currents in both directions (Figure 6b). The specific capacitance is 175 F/g at 5 mV/s in the potential range of 0−1 V for an electrode with a mass loading of 0.45 mg. Galvanostatic discharge plots at various current densities in a potential window of 1 V exhibit ideal linear behavior (Figure 6c). The specific capacitance is 160 F/g at a current density of 1 A/g and similar in magnitude to capacitance calculated from cyclic voltammograms. Galvanostatic charge/discharge plots at a current density of 1 A/g show ideally polarized electrode behavior, a reversible capacitance, and a linear potential change during charge/discharge cycles (Figure 6d). Increasing the current density by 3 orders of magnitude from 0.1 to 100 A/g shows a decrease in the specific capacitance from 165 to 150 F/g (Figure 6e). This slight change represents only a ∼9% decrease and indicates an excellent rate response. Furthermore, this supercapacitor is stable after 1000 charge/discharge cycles at a current density of 1 A/g and exhibits 94% capacitance retention (Figure 6f).

CONCLUSION

This study introduces a direct route to freestanding films of PEDOT nanofibers possessing high conductivity (130 S/cm) and leads to highly efficient nanofibrillar electrodes exhibiting a specific capacitance of 175 F/g. Deposition from the vapor phase leads to strong adhesion between the deposited coating and the current collector, resulting in a low internal resistance. By utilizing hard carbon fiber paper as the current collector, a three-dimensional architecture is homogeneously coated by nanofibers, thereby maximizing interfacial contact area for efficient supercapacitors. EVPP is simple, reproducible, and obviates the need for an extrinsic hard template, resulting in homogeneous, highly conductive, high aspect ratio one-dimensional nanoarchitectures. The oxidant $FeCl_3$ is commonly used for the synthesis of many types of conducting polymers and affords a chemical handle for developing EVPP into a universal deposition technique.

METHODS

Synthesis. High aspect ratio nanofibrillar PEDOT was deposited *via* evaporative vapor-phase polymerization inside a small chemical vapor deposition (CVD) chamber equipped with heaters and thermocouples connected to a PID controller for accurate and constant homogeneous heating. The CVD chamber's walls and lid were electrically heated to avoid condensation and allow reactant vapor to build up. The substrate was a 2×3 cm^2 piece of a gold-coated polyimide flexible tape (Astral Technology Unlimited, Inc.) and rested inside the CVD chamber. Typically, a 150 μL droplet of a 0.266 M aqueous solution of $FeCl_3$ (3.99×10^{-5} mol) was placed at the center of the flexible substrate. A chlorobenzene solution containing the monomer 3,4-ethylenedioxythiophene (EDOT) inside the CVD chamber was distributed in two glass reservoirs totaling 500 μL of a 0.0674 M (total number of moles = 6.74×10^{-5}). Then, the CVD chamber lid was closed and the temperature ramped up from 25 to 130 °C at approximately 400 °C/h and reached 130 °C after 12 min; the reaction was then kept at 130 °C for 33 min, making the total reaction time 45 min (Figure S2). The final EVPP-PEDOT film was dried at 130 °C for 30 min.

Characterization. *Four-Point Probe Conductivity Measurements.* Four-point probe conductivity was determined using a MMR Technologies Inc. Hall and van der Pauw measuring station. Spring-loaded gold probes contacted four electrodes 5 mm apart from each other arranged in a squared geometry; a thermally evaporated electrode was 1 mm × 1 mm × 500 nm.

Two-Point Probe Conductivity Measurements. Gold-coated patterned electrodes on SiO_2/Si were utilized for measurements of *I*−*V* curves. An EVPP-PEDOT film was purified and dried overnight and then analyzed *via* Gamry's Instruments electrochemical measurement system (PCI4 potentiostat/galvanostat) installed in a PC.

Film Thickness. The thickness of an EVPP-PEDOT film was measured by contact profilometry using a Veeco Dektak 150 surface profiler. Samples were washed in methanol and acid and dried. The edge of an EVPP-PEDOT film was anchored onto a silicon wafer with adhesive tape in order to hold samples during analysis.

Fabrication of PEDOT Supercapacitors. A PEDOT/PSS supercapacitor was produced from an aqueous suspension of commercially available poly(3,4-ethylenedioxythiophene)/poly(styrenesulfonate) (1.0 wt % in water, Sigma-Aldrich). The suspension was mixed with a polyvinylidene fluoride binder (90/10%) and sonicated for 30 min. This suspension was then coated onto a flexible gold-coated polyimide sheet and dried at 60 °C for 6 h in air and used as the electrodes. The weight of the active material in the electrode was calculated from the mass difference before and after coating using a high precision microbalance with a readability of 1 μg (Mettler Toledo, MX5). Celgard 3501 was used as a separator and 1.0 M tetrabutylammonium hexafluorophosphate in propylene carbonate as the electrolyte. On the other hand, the vapor-phase polymerization resulted in mechanically robust freestanding PEDOT films, which were directly used as supercapacitor electrodes without using polymer binders, conductive additives, or current collectors.

In an attempt to improve the electrochemical properties of this supercapacitor, EVPP-PEDOT was grown on top of a carbon current collector. Hard carbon fiber paper current collectors (Spectracarb 2050A, produced by Engineered Fibers Technology, with a surface area of 0.25−0.30 m^2/g) were flexible, mechanically robust, and cut with scissors into 8 mm × 50 mm sizes. Current collectors were rinsed in ethanol for 5 min, dried on a hot plate at 130 °C for 30 min, and masked with a thin film of 5 min epoxy that exposed bare carbon at the tip of the current collector (8 mm × 15 mm). After deposition, the electrodes were soaked for 12 h in an aqueous solution of 6 M HCl in order to remove reduced oxidant, and the weight of the active material was determined utilizing a TA Instruments' Discovery TGA microbalance with a 0.001 μg resolution. The electrochemical cell of the supercapacitor contained a 6 M HCl aqueous electrolyte and was fabricated with one layer of Celgard 3501 encased in a sealed Kapton tape electrolyte pocket. The potentiostat lead and the current collector were connected with silver colloidal paste and with a protective thick coat of 5 min epoxy that ensured electrical stability.

Electrochemical Measurements. All measurements were carried out on a VersaSTAT3 potentiostat/galvanostat (Princeton Applied Research), using a two-electrode configuration.

X-ray Photoelectron Spectroscopy. Analysis was carried out using an AXIS Ultra DLD, Kratos Analytical. Samples were dried on a hot plate at 130 °C for 30 min and dried inside a desiccator for 12 h prior to analysis. Note that EVPP-PEDOT is hydrophilic and can readily absorb moisture from the atmosphere.

Powder X-ray Diffraction. Phase identification was carried out on an EVPP-PEDOT film *via* an X'Pert Pro powder X-ray diffraction system (PANalytical, Netherlands) by utilizing a Cu Kα X-ray beam (λ = 1.5418 Å).

Raman Spectroscopy. Raman characterization was carried out using a Renishaw 1000 instrument, with a 50× objective lens, and peak fitting required using the instrument's software.

Conflict of Interest: The authors declare no competing financial interest.

Acknowledgment. This study was supported by the Dr. Martin Luther King Jr. Visiting Scholars Program, the Koch Institute for Integrative Cancer Research (NCI, grant 2P30CA014051-39), the Koch Institute's Peterson Nanotechnology Materials Core Facilities, and by the Institute for Soldier Nanotechnology facilities (U.S. Army Research Office, contract W911NF-07-D-0004) at the Massachusetts Institute of Technology. This work was also supported by Boeing (R.B.K.).

Supporting Information Available: Vapor-phase deposition strategies for non-nanostructured transparent PEDOT films, droplet evaporation modes, the role of water during the synthesis of PEDOT, the effect of removing excess iron chloride using methanol and acid, schematics of a vapor deposition chamber, graph showing the ramping temperature profile, SEM images of a wrinkled topography of vertically directed one-dimensional architectures, SEM images of a large-scale coverage of one-dimensional architectures; SEM images show evolution of one-dimensional architectures; SEM images and XRD patterns of the cross section of an EVPP-PEDOT film, digital images show inside of the CVD chamber; SEM images show the radial inward deposition of nanostructures, SEM images of the initial morphologies present during polymerization, SEM images of the effect of water on nanoscale morphology, EDS elemental maps demonstrating the templated growth of one-dimensional architectures of EVPP-PEDOT, and SEM images showing the effect of template removal on nanoscale morphology. This material is available free of charge *via* the Internet at http://pubs.acs.org.

REFERENCES AND NOTES

1. Simon, P.; Gogotsi, Y. Materials for Electrochemical Capacitors. *Nat. Mater.* **2008**, *7*, 845–854.
2. Yang, Y.; Zhang, L.; Li, S.; Yang, W.; Xu, J.; Jiang, Y.; Wen, J. Electrochemical Performance of Conducting Polymer and Its Nanocomposites Prepared by Chemical Vapor Phase Polymerization Method. *J. Mater. Sci.: Mater. Electron.* **2013**, *24*, 2245–2253.
3. Pandey, G. P.; Rastogi, A. C.; Westgate, C. R. All-Solid-State Supercapacitors with Poly(3,4-ethylenedioxythiophene)-Coated Carbon Fiber Paper Electrodes and Ionic Liquid Gel Polymer Electrolyte. *J. Power Sources* **2014**, *245*, 857–865.
4. Hsu, Y.-K.; Chen, Y.-C.; Lin, Y.-G.; Chen, L.-C.; Chen, K.-H. Direct-Growth of Poly(3,4-ethylenedioxythiophene) Nanowires/Carbon Cloth as Hierarchical Supercapacitor Electrode in Neutral Aqueous Solution. *J. Power Sources* **2013**, *242*, 718–724.
5. Patra, S.; Munichandraiah, N. Supercapacitor Studies of Electrochemically Deposited PEDOT on Stainless Steel Substrate. *J. Appl. Polym. Sci.* **2007**, *106*, 1160–1171.
6. Liu, R.; Cho, S. I.; Lee, S. B. Poly(3,4-ethylenedioxythiophene) Nanotubes as Electrode Materials for a High-Powered Supercapacitor. *Nanotechnology* **2008**, *19*, 215710–215717.
7. Kim, J.-Y.; Kwon, M.-H.; Min, Y.-K.; Kwon, S.; Ihm, D.-W. Self-Assembly and Crystalline Growth of Poly(3,4-ethylenedioxythiophene) Nanofilms. *Adv. Mater.* **2007**, *19*, 3501–3506.
8. Aradilla, D.; Estrany, F.; Armelin, E.; Alemán, C. Ultraporous Poly(3,4-ethylenedioxythiophene) for Nanometric Electrochemical Supercapacitor. *Thin Solid Films* **2012**, *520*, 4402–4409.
9. Xie, X. N.; Wang, J.; Lee, K. K.; Loh, K. P. Supercapacitive Energy Storage Based on Ion-Conducting Channels in Hydrophilized Organic Network. *J. Polym. Sci., Part B: Polym. Phys.* **2011**, *49*, 1234–1240.
10. Gogotsi, Y.; Simon, P. True Performance Metrics in Electrochemical Energy Storage. *Science* **2011**, *334*, 917–918.
11. Laforgue, A. All-Textile Flexible Supercapacitors Using Electrospun Poly(3,4-ethylenedioxythiophene) Nanofibers. *J. Power Sources* **2011**, *196*, 559–564.
12. Im, S. G.; Gleason, K. K. Systematic Control of the Electrical Conductivity of Poly(3,4-ethylenedioxythiophene) *via* Oxidative Chemical Vapor Deposition. *Macromolecules* **2007**, *40*, 6552–6556.
13. Winther-Jensen, O.; Desai, S.; Shepherd, R. L.; Innis, P. C.; Winther-Jensen, B.; Forsyth, M.; Wallace, G. G.; MacFarlane, D. R. Ion Effects in Redox Cycling of Conducting Polymer Based Electrochromic Materials. *Electrochem. Commun.* **2010**, *12*, 1505–1508.
14. Mozer, A. J.; Panda, D. K.; Gambhir, S.; Romeo, T. C.; Winther-Jensen, B.; Wallace, G. G. Flexible and Compressible Goretex–PEDOT Membrane Electrodes for Solid-State Dye-Sensitized Solar Cells. *Langmuir* **2009**, *26*, 1452–1455.
15. Chen, C.-C.; Dou, L.; Zhu, R.; Chung, C.-H.; Song, T.-B.; Zheng, Y. B.; Hawks, S.; Li, G.; Weiss, P. S.; Yang, Y. Visibly Transparent Polymer Solar Cells Produced by Solution Processing. *ACS Nano* **2012**, *6*, 7185–7190.
16. Winther-Jensen, B.; Winther-Jensen, O.; Forsyth, M.; Macfarlane, D. R. High Rates of Oxygen Reduction over a Vapor Phase-Polymerized PEDOT Electrode. *Science* **2008**, *321*, 671–674.
17. Cao, Y.; Kovalev, A. E.; Xiao, R.; Kim, J.; Mayer, T. S.; Mallouk, T. E. Electrical Transport and Chemical Sensing Properties of Individual Conducting Polymer Nanowires. *Nano Lett.* **2008**, *8*, 4653–4658.
18. Im, S. G.; Kusters, D.; Choi, W.; Baxamusa, S. H.; van de Sanden, M. C. M.; Gleason, K. K. Conformal Coverage of Poly(3,4-ethylenedioxythiophene) Films with Tunable Nanoporosity *via* Oxidative Chemical Vapor Deposition. *ACS Nano* **2008**, *2*, 1959–1967.
19. Martin, D. C.; Wu, J.; Shaw, C. M.; King, Z.; Spanninga, S. A.; Richardson-Burns, S.; Hendricks, J.; Yang, J. The Morphology of Poly(3,4-ethylenedioxythiophene). *Polym. Rev.* **2010**, *50*, 340–384.
20. Lee, J. A.; Shin, M. K.; Kim, S. H.; Kim, S. J.; Spinks, G. M.; Wallace, G. G.; Ovalle-Robles, R.; Lima, M. D.; Kozlov, M. E.; Baughman, R. H. Hybrid Nanomembranes for High Power and High Energy Density Supercapacitors and Their Yarn Application. *ACS Nano* **2011**, *6*, 327–334.
21. Trujillo, N. J.; Barr, M. C.; Im, S. G.; Gleason, K. K. Oxidative Chemical Vapor Deposition (oCVD) of Patterned and Functional Grafted Conducting Polymer Nanostructures. *J. Mater. Chem.* **2010**, *20*, 3968–3972.
22. Bhattacharyya, D.; Yang, R.; Gleason, K. K. High Aspect Ratio, Functionalizable Conducting Copolymer Nanobundles. *J. Mater. Chem.* **2012**, *22*, 17147–17152.
23. Laforgue, A.; Robitaille, L. Deposition of Ultrathin Coatings of Polypyrrole and Poly(3,4-ethylenedioxythiophene) onto Electrospun Nanofibers Using a Vapor-Phase Polymerization Method. *Chem. Mater.* **2010**, *22*, 2474–2480.
24. Kwon, O. S.; Park, E.; Kweon, O. Y.; Park, S. J.; Jang, J. Novel Flexible Chemical Gas Sensor Based on Poly(3,4-ethylenedioxythiophene) Nanotube Membrane. *Talanta* **2010**, *82*, 1338–1343.
25. Yang, X.-M.; Shang, S.-M.; Li, L.; Tao, X.-M.; Yan, F. Vapor Phase Polymerization of 3,4-ethylenedioxythiophene on Flexible Substrate and Its Application on Heat Generation. *Polym. Adv. Technol.* **2011**, *22*, 1049–1055.
26. Fabretto, M.; Zuber, K.; Hall, C.; Murphy, P.; Griesser, H. J. The Role of Water in the Synthesis and Performance of Vapour Phase Polymerised PEDOT Electrochromic Devices. *J. Mater. Chem.* **2009**, *19*, 7871–7878.

27. Chelawat, H.; Vaddiraju, S.; Gleason, K. Conformal, Conducting Poly(3,4-ethylenedioxythiophene) Thin Films Deposited Using Bromine as the Oxidant in a Completely Dry Oxidative Chemical Vapor Deposition Process. *Chem. Mater.* **2010**, *22*, 2864–2868.
28. Jang, K.-S.; Kim, D. O.; Lee, J.-H.; Hong, S.-C.; Lee, T.-W.; Lee, Y.; Nam, J.-D. Synchronous Vapor-Phase Polymerization of Poly(3,4-ethylenedioxythiophene) and Poly(3-hexylthiophene) Copolymer Systems for Tunable Optoelectronic Properties. *Org. Electron.* **2010**, *11*, 1668–1675.
29. Kim, T.-W.; Woo, H.-Y.; Jung, W.-G.; Ihm, D.-W.; Kim, J.-Y. On the Mechanism of Conductivity Enhancement in Plasma Treated Poly(3,4-ethylenedioxythiophene) Films. *Thin Solid Films* **2009**, *517*, 4147–4151.
30. Zou, R.; Guo, X.; Yang, J.; Li, D.; Peng, F.; Zhang, L.; Wang, H.; Yu, H. Selective Etching of Gold Nanorods by Ferric Chloride at Room Temperature. *CrystEngComm* **2009**, *11*, 2797–2803.
31. Yang, D.-Q.; Sacher, E. Core/Shell Formation of Gold Nanoparticles Induced on Exposure to *N*,*N*-Dimethylformamide: Chemical and Morphological Changes. *J. Phys. Chem. C* **2007**, *111*, 14320–14326.
32. Deegan, R. D. Pattern Formation in Drying Drops. *Phys. Rev. E* **2000**, *61*, 475–485.
33. Winther-Jensen, B.; Forsyth, M.; West, K.; Andreasen, J. W.; Bayley, P.; Pas, S.; MacFarlane, D. R. Order-Disorder Transitions in Poly(3,4-ethylenedioxythiophene). *Polymer* **2008**, *49*, 481–487.
34. Subramanian, P.; Clark, N.; Winther-Jensen, B.; MacFarlane, D.; Spiccia, L. Vapour-Phase Polymerization of Pyrrole and 3,4-Ethylenedioxythiophene Using Iron(III) 2,4,6-Trimethylbenzenesulfonate. *Aust. J. Chem.* **2009**, *62*, 133–139.
35. Winther-Jensen, B.; West, K. Vapor-Phase Polymerization of 3,4-Ethylenedioxythiophene: A Route to Highly Conducting Polymer Surface Layers. *Macromolecules* **2004**, *37*, 4538–4543.
36. Bubnova, O.; Khan, Z. U.; Malti, A.; Braun, S.; Fahlman, M.; Berggren, M.; Crispin, X. Optimization of the Thermoelectric Figure of Merit in the Conducting Polymer Poly(3,4-ethylenedioxythiophene). *Nat. Mater.* **2011**, *10*, 429–433.
37. Dou, L.; You, J.; Yang, J.; Chen, C.-C.; He, Y.; Murase, S.; Moriarty, T.; Emery, K.; Li, G.; Yang, Y. Tandem Polymer Solar Cells Featuring a Spectrally Matched Low-Bandgap Polymer. *Nat. Photonics* **2012**, *6*, 180–185.
38. Yang, Y.; Yu, G.; Cha, J. J.; Wu, H.; Vosgueritchian, M.; Yao, Y.; Bao, Z.; Cui, Y. Improving the Performance of Lithium–Sulfur Batteries by Conductive Polymer Coating. *ACS Nano* **2011**, *5*, 9187–9193.
39. El-Kady, M. F.; Strong, V.; Dubin, S.; Kaner, R. B. Laser Scribing of High-Performance and Flexible Graphene-Based Electrochemical Capacitors. *Science* **2012**, *335*, 1326–1330.